Title

SF3B1 thermostability as an assay for splicing inhibitor interactions.

Journal

Journal of Biological Chemistry, 301(2)

Authors

Amorello, Angela

Chandrashekar Reddy, Guddeti

Melillo, Bruno

et al.

Publication Date

2024-12-24

DOI

10.1016/j.jbc.2024.108135

Peer reviewed

SF3B1 thermostability as an assay for splicing inhibitor interactions

Received for publication, December 19, 2023, and in revised form, November 16, 2024 Published, Papers in Press, December 24, 2024,
https://doi.org/10.1016/j.jbc.2024.108135

Angela N. Amorello[1], Guddeti Chandrashekar Reddy[2], Bruno Melillo[3], Benjamin F. Cravatt[3], Arun K. Ghosh[2], and Melissa S. Jurica[4,5,*]

From the [1]Department of Chemistry and Biochemistry, University of California, Santa Cruz, California, USA; [2]Department of Chemistry and Department of Medicinal Chemistry, Purdue University, West Lafayette, Indiana, USA; [3]Department of Chemistry, Scripps Research, La Jolla, California, USA; [4]Department of Molecular Cell and Developmental Biology, University of California, Santa Cruz, California, USA; and [5]Center for Molecular Biology of RNA, University of California, Santa Cruz, California, USA

Reviewed by members of the JBC Editorial Board. Edited by Ronald Wek

The spliceosome protein, SF3B1, is associated with U2 snRNP during early spliceosome assembly for pre-mRNA splicing. Frequent somatic mutations in SF3B1 observed in cancer necessitates the characterization of its role in identifying the branchpoint adenosine of introns. Remarkably, SF3B1 is the target of three distinct natural product drugs, each identified by their potent anti-tumor properties. Structural studies indicate that SF3B1 conformational flexibility is functionally important, and suggest that drug binding blocks the transition to a closed state of SF3B1 required for the next stage of spliceosome assembly. This model is confounded, however, by the antagonistic property of an inactive herboxidiene analog. In this study, we established an assay for evaluating the thermostability of SF3B1 present in the nuclear extract preparations employed for *in vitro* splicing studies, to investigate inhibitor interactions with SF3B1 in a functional context. We show that both active and antagonistic analogs of natural product inhibitors affect SF3B1 thermostability, consistent with binding alone being insufficient to impair SF3B1 function. Surprisingly, SF3B1 thermostability differs among nuclear extract preparations, likely reflecting its conformational status. We also investigated a synthetic SF3B1 ligand, WX-02-23, and found that it increases SF3B1 thermostability and interferes with *in vitro* splicing by a mechanism that strongly resembles the activity of natural product inhibitors. We propose that altered SF3B1 thermostability can serve as an indicator of inhibitor binding to complement functional assays of their general effect on splicing. It may also provide a means to investigate the factors that influence SF3B1 conformation.

Splicing factor 3B (SF3B) is a multiprotein complex that functions with the U2 small nuclear ribonucleoprotein (U2 snRNP) to recognize the branchpoint adenosine of introns during pre-messenger RNA splicing (1). This recognition event is important because the adenosine directly participates in splicing chemistry and influences the choice of the 3′ splice that defines the intron-exon boundary. The largest SF3B protein, SF3B1, frequently acquires specific somatic mutations in a variety of cancers (2–5), which lead to altered selection of branchpoints and 3′ splice site usage in several gene transcripts (6, 7). Efforts to link SF3B1 mutation to oncogenesis are ongoing. For example, the most frequently occurring SF3B1 mutation, SF3B1^{K700E}, contributes to MYC hyperactivation *via* aberrant splicing of protein phosphatase 2A (PP2A) subunit PPP2R5A (8).

SF3B1 is also the target of three distinct families of natural products first identified for their potent cytotoxicity and anti-tumor activity, and exemplified by pladienolide B, herboxidiene, and spliceostatin A (SSA) (9–14). The compounds, collectively known as SF3B1 inhibitors, interfere with U2 snRNP's engagement with the intron during spliceosome assembly (15–18). SF3B1 inhibitors have garnered much interest for their potential as cancer therapeutics due to their potent toxicity to cancer cells and capacity to reduce tumor volumes in patient-derived xenografts (9, 10, 14). Furthermore, cells carrying SF3B1 cancer mutations exhibit even higher sensitivity to the compounds (19, 20). Pladienolide B analog H3B-8800 is currently in clinical trials (20), https://clinicaltrials.gov/ct2/show/NCT02841540. While a significant clinical response has not been reported, some results for patients with myelodysplastic syndrome (MDS) appear to be promising (21). A better understanding of how the different inhibitors impact SF3B1 function is needed to support their further development for clinical use.

Recent structural studies provide some clues to the SF3B1 inhibitor mechanism. The large HEAT-repeat domain of SF3B1 has a conformationally flexible C-shape that appears to mediate the role of the protein in branchpoint recognition and inhibitor action (22). Prior to engaging with an intron, the domain is observed with an open conformation (23). After intron engagement, the domain closes so that SF3B1 essentially clamps the duplex formed by U2 snRNA and intron base pairing (24–26). The closed conformation also sandwiches the branchpoint adenosine of the intron in a space between SF3B1 HEAT-repeats 15 and 16, a state that appears to be required as a signal for further spliceosome assembly. Structures of a minimalized SF3B complex bound to the pladienolide B analog

* For correspondence: Melissa S. Jurica, mjurica@ucsc.edu.

E7107 and an SSA-stalled spliceosome display SF3B1 in the open conformation. The diene functionality common among the different inhibitor structures is situated in a tunnel-like cavity between SF3B1 HEAT-repeat 15 and a partner protein PHF5A (27–29). For SF3B1 closing, residues that contribute to the drug cavity must move to contact the intron branchpoint adenosine. The inhibitors are proposed to interfere with splicing by both steric blocking of the branchpoint adenosine binding site and stabilization of the open conformation.

Whether and how SF3B1 conformation is regulated is not currently known. Working under the assumption that inhibitor binding depends on the open conformation, we concluded that higher temperature and an ATP-dependent activity influence accessibility of the binding pocket, suggesting the "ground state" is closed (30). In the context of U2 snRNP, interactions with U2 snRNA as well as the proteins HTATSF1 and RNA-dependent ATPase DDX46, the human ortholog of yeast Prp5p, appear to stabilize the open conformation of SF3B1 (23). One possibility is that the open conformation represents an activated state of U2 snRNP necessary for intron binding. Similarly, SF3B1 closing may be regulated by DDX46, which has a role in determining the fidelity of branch helix formation (31, 32).

Through structure-function analysis of the SF3B1 inhibitor herboxidiene, we showed that a carboxymethyl substitution at a position predicted to interact with charged residues in HEAT-repeat 15 results in an inactive analog (iHB) with no effect on splicing. Surprisingly, the iHB analog antagonizes the splicing inhibitory activity of the parent compound, pladienolide B and SSA, which suggests that antagonism is mediated by competitive binding to SF3B1 (16, 30). This supposition conflicts with the steric model of SF3B1 inhibitor action posed above because the apparent binding of the iHB analog does not interfere with SF3B1 function. Instead, we hypothesize that the signal allowing for SF3B1 closure over an intron may be impaired by a key drug interaction that is lacking with iHB. One caveat to our model, however, is that we used completion of splicing as an indirect measure of inhibitor binding.

In searching for a more direct measurement of SF3B1 interactions with different analogs, we considered other reported strategies using isolated SF3B complex (20, 33). However, because SF3B1 interactions with RNA and proteins in U2 snRNP impact the conformation of the protein and binding pocket, we were concerned that an important context for drug interactions would be missing. Unfortunately, the biogenesis of U2 snRNP is complex, and it cannot be reconstituted. We therefore turned to the cellular thermal shift assay (CETSA) developed to provide information about drug binding to a target protein in cells (34, 35). We aimed to evaluate splicing inhibitor interactions with native SF3B1 in the nuclear extract employed for most studies of splicing and spliceosome function (36). Employing a dot blot strategy to compare the amount of soluble SF3B1 after exposing nuclear extract to increasing temperatures, we show that SF3B1 inhibitors induce a small, but consistent increase in SF3B1 thermostability in HeLa nuclear extracts that supports *in vitro* splicing. Surprisingly, we find that SF3B1 in some extract preparations is significantly less thermostable, and the subsequent stabilizing impact of inhibitors is much greater. Low SF3B1 thermostability correlates with poor splicing activity in the extract, and we speculate that it may reflect SF3B1 functional interactions with U2 snRNP. The iHB analog also increases SF3B1 thermostability, which is consistent with competitive binding mediating the antagonism of active inhibitors. Finally, we used the assay to investigate a synthetic ligand reported to covalently target SF3B1 on a cysteine in HEAT-repeat 16 adjacent to the drug binding pocket (37). Despite a very different chemical structure, this compound also increases SF3B1 thermostability and interferes with the assembly of the spliceosome on an intron like the natural product inhibitors. Together our results indicate the SF3B1 thermal shift assay is a useful complement to functional splicing assays for investigating drug interaction with SF3B1 and for exploring conditions that impact SF3B1 conformation and function in splicing.

Results

Impact of an SSA analog on the thermostability of SF3B1 in nuclear extract

To determine the thermostability profile of SF3B1 in the HeLa cell nuclear extract commonly used for *in vitro* splicing analysis and the potential impact of SF3B1 inhibitors, we incubated 5 μM SSA analog SSA-917 with nuclear extract. This concentration is ∼50-fold higher than its IC_{50} for splicing inhibition. Aliquots of the mixture were then exposed to a range of increasing temperatures, and then centrifuged to remove denatured proteins. We initially used western blots to assess the amount of soluble SF3B1 (Fig. 1*B*). As expected, the predominant SF3B1 band showed decreased intensity with increasing temperature (Fig. 1*A*). In the SSA-917 treated extract, the amount of SF3B1 appeared to be higher relative to the DMSO control at intermediate temperatures, consistent with drug binding providing a measure of stabilization with heat denaturation. A non-linear regression to relative band intensities from replicate samples and blots was used to determine the temperature where half of the total SF3B1 is denatured (T_m) (Fig. 1*C*). The value for SSA-917 treatment was slightly higher (53.1 vs 54.5 °C) than with DMSO, but a 95% confidence interval could not be determined, and we could therefore not test for statistical significance.

Because of the large number of samples that need to be analyzed in parallel, ideally on the same blot, we turned to dot blotting to analyze both experimental and technical replicates on the same blot and to add another temperature point. First, we established that serial dilution of nuclear extract applied directly to a membrane resulted in a linear decrease of SF3B1 immunosignal (Fig. 1*D*-left). SF3B1 immunosignal of 45 identical samples across a dot blot exhibits a 10.4% coefficient of variation (Fig. 1*D*). Relative dot blot intensities of the same samples analyzed by Western blot yields a similar denaturation profile, and, with an extra temperature point and technical replicate, we were able to determine that the small difference in T_m value for SSA-917 (54.6) and DMSO (53.4) has statistical significance (p = 0.0073).

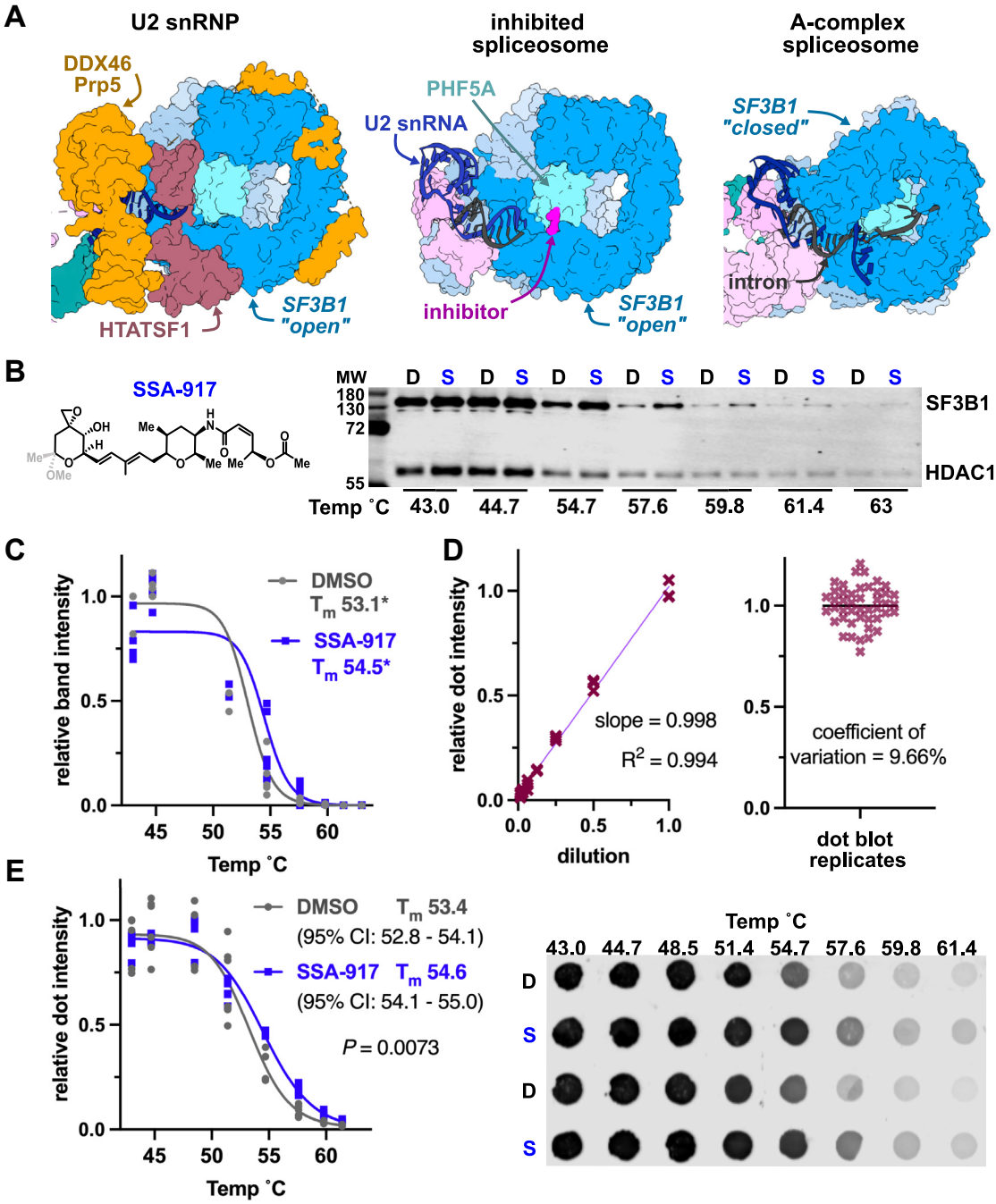

Figure 1. A SSA analog increases SF3B1 thermostability in nuclear extract. *A*, SF3B1 interactions and conformation differ significantly between cryo-EM models of 17S U2 snRNP (6Y50), SSA-inhibited spliceosome (7ONB), and A-complex spliceosome (6G9O). *B*, the chemical structure of SSA-917, which lacks the C1 methyl and O-methyl groups of SSA (shown in *gray*), next to representative Western blot probed with anti-SF3B1 and anti-HDAC1. Gels were loaded with the soluble fraction of HeLa nuclear extract first incubated with 5 μM SSA-917 or carrier DMSO and then exposed to the indicated temperature. Anti-HDAC1 signal serves as a loading control. *C*, relative anti-SF3B1 band intensity vs temperature of heat treatment for replicate samples with replicate blots. The data are fit to a non-linear regression model to derive T_m values (*complete confidence interval could not be determined). *D*, the *left* graph shows relative anti-SF3B1 dot blot signal vs. triplicate samples of serially diluted nuclear extract fit to linear regression. The *right* graph shows the distribution of the anti-SF3B1 signal for identical samples loaded on a single dot blot (n = 45) relative to the average signal with the associated coefficient of variance. *E*, relative anti-SF3B1 dot blot signal of the same replicate samples shown in (*B*) vs temperature of heat treatment. Data from triplicate dot blot measurements are fit to a non-linear regression model to derive T_m values, which were compared using the extra sum-of-squares F-test to determine significance. A portion of the dot blot is shown to the *right*. SSA, spliceostatin A.

An unknown factor affects SF3B1 thermostability in some nuclear extract preparations

Nuclear extracts are prepared in batches from liter-scale cultures of HeLa extracts and exhibit batch to batch variability in terms of 260/280 UV absorbance levels and *in vitro* splicing efficiency, including cases of completely "dead" extract. The extract used for Figure 1 (NE-1), exhibits relatively good splicing efficiency and higher UV absorbance.

Impact of splicing inhibitors on SF3B1 thermostability

To determine if the effect of SSA on SF3B1 is consistent across nuclear extracts preparation, we repeated the experiment with two additional nuclear extract preparations (NE-2 and NE-3). With NE-2, SSA increased the T_m of SF3B1 thermodenaturation by a little over 1 °C, with a thermostability profile like NE-1 (Fig. 2*A*). In contrast, NE-3 exhibited a very different pattern of SF3B1 thermostability. First, in the absence of inhibitor, the T_m of SF3B1 thermodenaturation is ~3 °C lower than NE-1 and NE-2. Second, the effect of SSA-917 is much more pronounced with a thermostability profile that cannot be fit by linear regression (Fig. 2*B*). To compare the behavior of additional extracts, we examined temperatures near the inflection points of the SF3B1 thermodenaturation curve. Figure 2*C* shows relative dot intensities at 40, 50 and 54 °C for NE-2, NE-3 and three additional extract preparations. Both NE-2 and NE-4 exhibit relatively high amounts of SF3B1 at 54 °C in DMSO, which increases slightly with SSA-917 treatment. In contrast, only a small amount of SF3B1 remains soluble at 54 °C with NE-3, NE-5, NE-6 (55 °C for NE-6) in DMSO. Strikingly, SSA-917 treatment significantly increases the portion of soluble SF3B1 to approximately the same level.

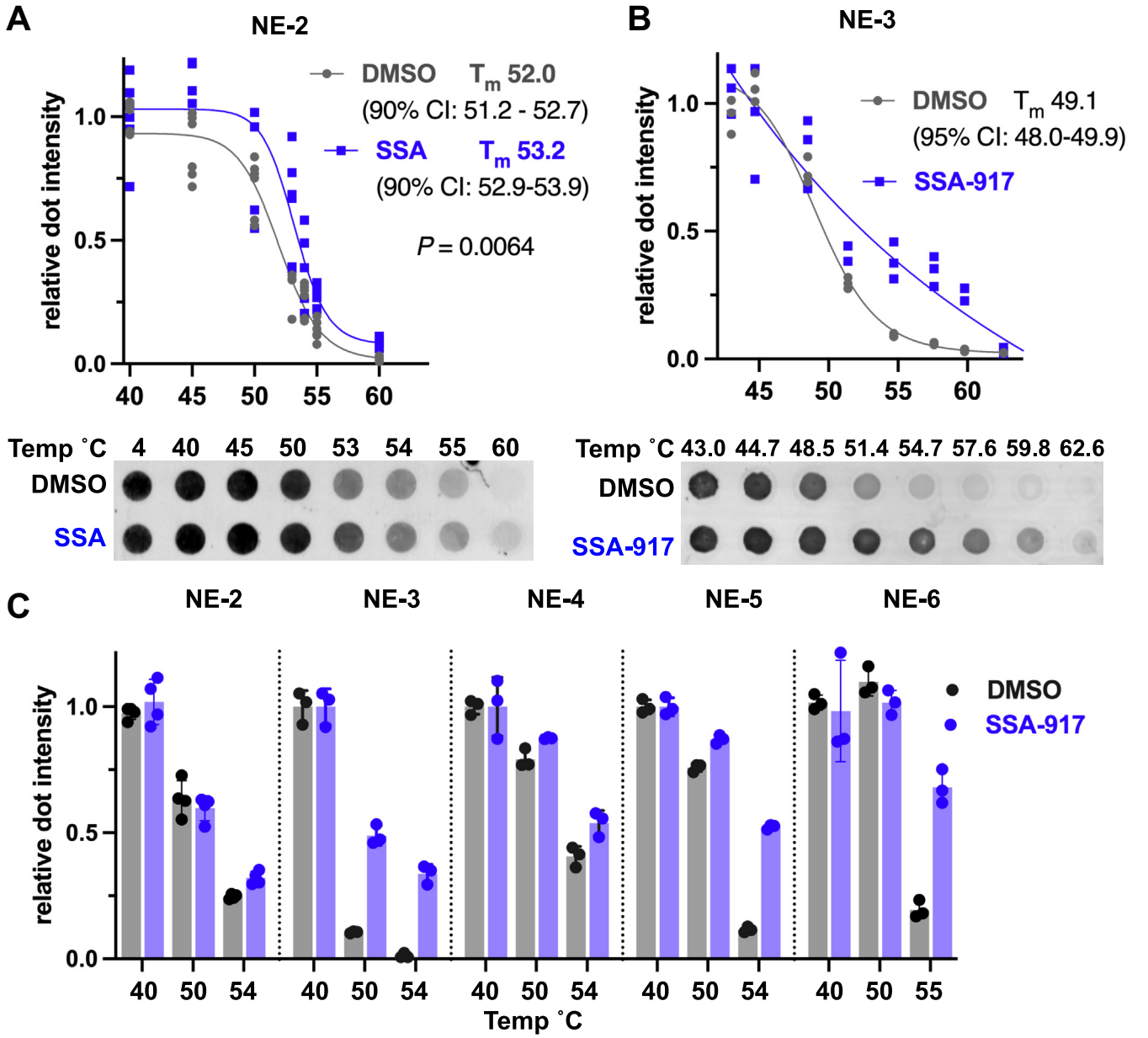

Figure 2. SSA overcomes extract intrinsic factors affecting SF3B1 thermostability. *A* and *B*, relative anti-SF3B1 dot blot signal for the soluble fraction of different nuclear extract preparation (NE-2 and NE-3) prepared and analyzed the same as described for Figure 1*E*. For NE-3 treated with 5 μM SSA-917, a T_m value could not be determined from the curve fit. One sample replicate from the correlating dot blot is shown below the graph. *C*, comparison of relative anti-SF3B1 dot intensities for soluble fractions of different nuclear extract preparations treated with DMSO or 5 μM SSA-917 and incubated at the indicated temperatures. SSA, spliceostatin A.

The molecular basis of this differential thermostability of SF3B1 is not clear at this point. NE-1, NE-2, and NE-4 have relatively high 260/280 nm UV absorbance and exhibit better splicing efficiency. NE-3 and NE-5 have lower 260/280 nm UV absorbance and exhibit little to no splicing efficiency, while NE-6 has intermediate 260/280 nm UV absorbance and slightly better splicing. Although we adjusted NE concentration to achieve similar UV absorbance for the extracts tested (for example NE-1 and NE-2 were tested at 50%, and NE-3 tested at 95% extract) overall protein/nucleic acid levels have the potential to affect thermostability. We therefore compared thermostability profiles of dilutions of NE-1 and NE-3 with and without SSA treatment. Each dilution of NE-1 slightly increases the T_m of SF3B1 with DMSO, but SSA treatment still provides a small boost in thermostability (Fig. 3*A*). NE-3 dilution decreased the T_m of SF3B1 in DMSO, but SSA treatment still greatly increases soluble SF3B1 in a pattern that cannot be fit by linear regression. These results, summarized in Figure 3*B*, show that protein/nucleic acid concentration is a relevant factor, but it does not account for the unusual thermostability of SF3B1 in NE-3.

There is a correlation between splicing efficiency and SF3B1 thermostability in that all extracts with lower SF3B1 thermostability have poor or no splicing capacity. However, the corollary does not hold. We tested four additional extracts, two with good splicing efficiency and two with splicing activity. The amount of soluble SF3B1 remaining after heating 40, 50 and 55 °C were very similar to each other and NE-1 (Fig. 3*C*).

Modulation of SF3B1 stability by other natural product scaffolds

One goal of developing an SF3B1 thermostability assay was to compare the effect of inhibitors and analogs on splicing efficiency with a complementary assessment of the interactions between the compounds and SF3B1 in nuclear extract. We therefore next used the assay with pladienolide B, herboxidiene, and a herboxidiene analog (iHB) that antagonizes the effect of active compounds (16, 30) (Fig. 4*A*). To more readily compare their ability to affect SF3B1 thermostability in different extracts we again analyzed the soluble fraction of after heating to 40, 50 and 54 °C. With NE-2, pladienolide B treatment produced a very small increase in soluble SF3B1 levels at 54 °C, while the effect of herboxidiene was not statistically significant (Fig. 4*C*). In NE-3, however, both compounds strongly increased SF3B1 thermostability at 50 and 54 °C (Fig. 4, *B* and *C*). These results suggest that similar interactions between SF3B1 and the three different natural product scaffolds are responsible for the increased SF3B1 thermostability. Notably, iHB also affects SF3B1 thermostability in NE-3 and NE-5 (Fig. 4, *B* and *C*). This result lends further support to our hypothesis that antagonism by iHB is mediated by competitive binding to SF3B1.

WX-02-23 shifts SF3B1 thermostability and inhibits pre-mRNA splicing in vitro

The Cravatt group reported a synthetic chemical ligand (WX-02-23) that covalently attaches to SF3B1 through cysteine 1111 and an inactive/non-competitive enantiomer

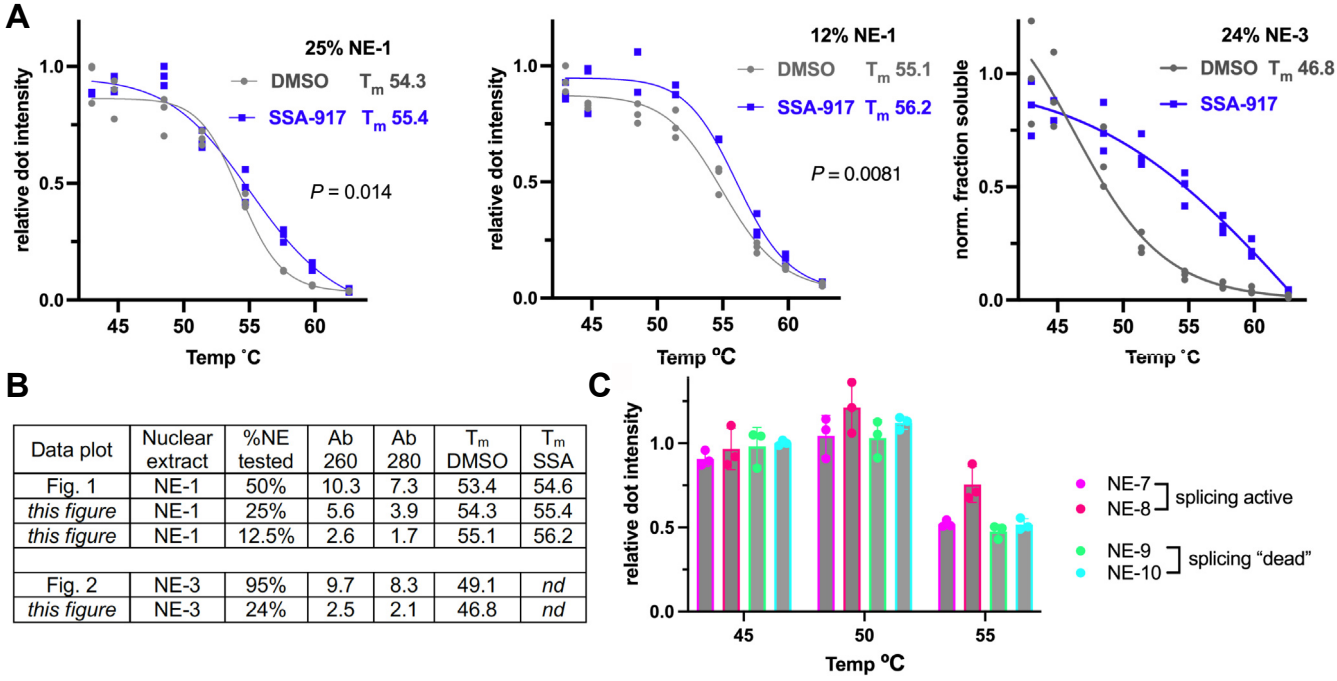

Data plot	Nuclear extract	%NE tested	Ab 260	Ab 280	T_m DMSO	T_m SSA
Fig. 1	NE-1	50%	10.3	7.3	53.4	54.6
this figure	NE-1	25%	5.6	3.9	54.3	55.4
this figure	NE-1	12.5%	2.6	1.7	55.1	56.2
Fig. 2	NE-3	95%	9.7	8.3	49.1	*nd*
this figure	NE-3	24%	2.5	2.1	46.8	*nd*

Figure 3. The concentration of nuclear extract does not account for differential thermostability of SF3B1. *A*, relative anti-SF3B1 dot blot signal for the soluble fraction of dilutions of NE-1 and NE-3 prepared and analyzed the same as described in Figure 1*E*. *B*, comparison of UV absorbance and T_m values for the extract dilutions tested. *C*, comparison of SF3B1 thermostability among extracts with robust or poor splicing activity.

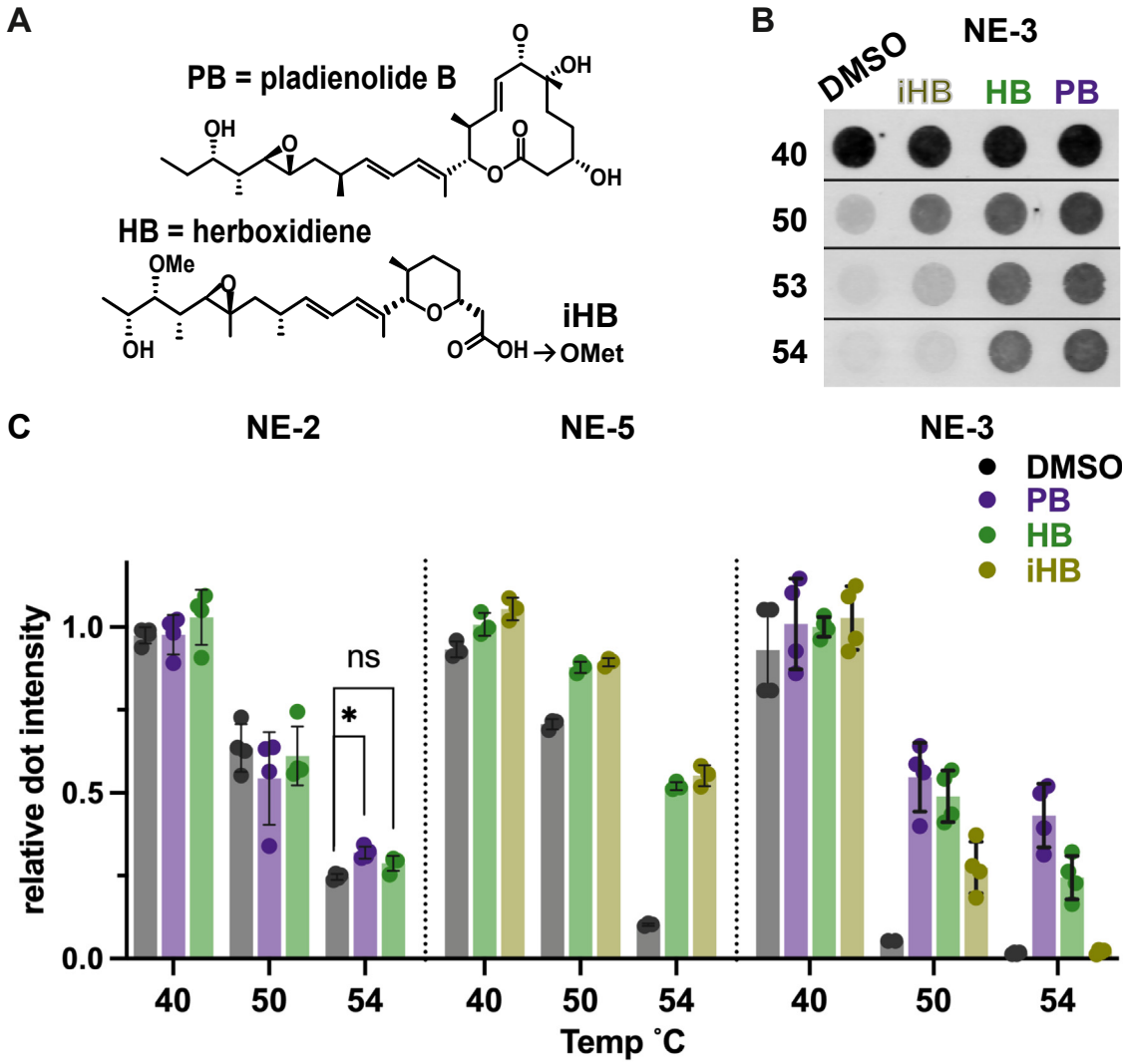

Figure 4. SF3B1 thermostability is affected by structurally distinct inhibitors and an inactive antagonist. *A*, the chemical structures of pladienolide B (PB) and herboxidiene (HB). The conversion of HB's C1 carboxyl to carboxymethyl yields the inactive antagonist iHB. *B*, representative dot blot showing anti-SF3B1 signal for the soluble fraction of NE-3 treated with 5 μM PB, 5 μM HB or 100 μM iHB and then heated at different temperatures. *C*, comparison of relative anti-SF3B1 dot intensities for soluble fractions of different nuclear extract preparations incubated with same concentration of the indicated compound as in B and then heated to 40, 50 or 54 °C. For NE-2, only PB treatment produced a significant increase in the amount of soluble SF3B1 at 54 °C (p = 0.0004).

(WX-02-43) (37) (Fig. 5*A*). In SF3B1, cysteine 1111 faces into the binding channel of the natural product splicing inhibitors, and pladienolide B was shown to compete with WX-02 to 23's interaction with SF3B1. Although the compound can influence splicing in cells, the question of its effect on SF3B1 function was not fully answered.

To determine whether WX-02-23 interferes with U2 snRNP's engagement with an intron in a way that reduces spliceosome assembly and subsequent catalysis of splicing chemistry, we tested its effect in the *in vitro* splicing system. Inclusion of WX-02-23 results in loss of both first and second step splicing products with an IC_{50} of ~5 μM, while WX-02-43 has no effect (Fig. 4*B*). Notably, an A-like complex similar to that induced by SSA-917 accumulates in the presence of WX-02-23, with no further complex formation (Fig. 4*C*). Together, these results are consistent with the idea that molecules with very different structures nonetheless interfere with SF3B1's role in spliceosome assembly in the same manner.

Next, we used the dot blot assay to test whether WX-02-23 also influences SF3B1 thermostability (Fig. 5*B*). While the impact of WX-02-23 does not reach statistical significance in NE-6 like SSA-917, the compound robustly increased the amount of soluble SF3B1 in NE-3 at 50 and 54 °C. This result further supports the model that ligation of WX-02-23 to SF3B1 mimics binding of the natural product splicing inhibitors. As expected, WX-02-43 had no effect on SF3B1 thermostability in NE-6. It did increase the amount of soluble SF3B1 in NE-1 at 50 °C, suggesting that it although it does not react with cysteine 1111, it may interact with SF3B1 to some extent.

WX-02-23 was shown to stabilize the association of DDX42 with SF3B1, which invited the suggestion that the compound

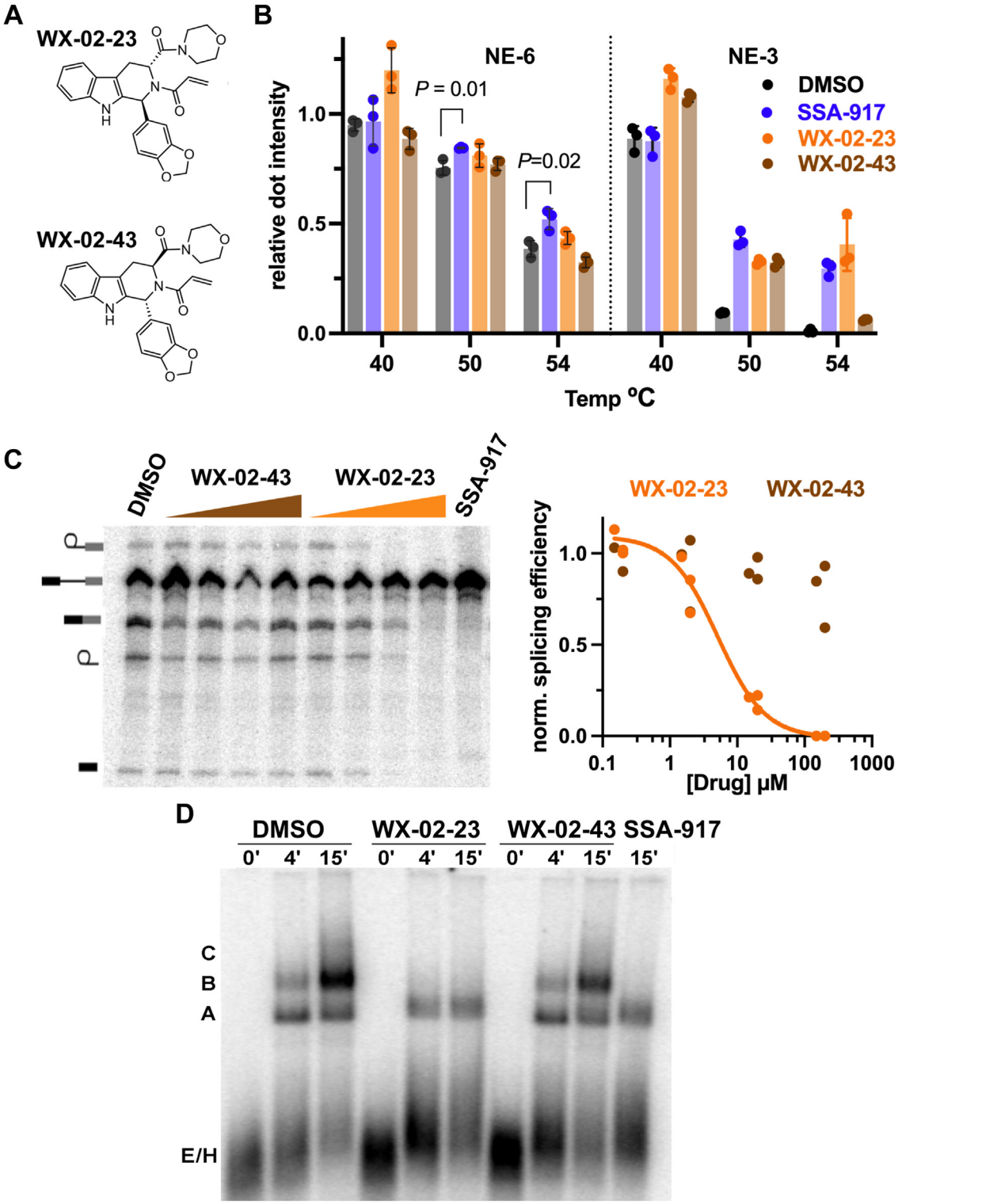

Figure 5. The synthetic covalent ligand WX-02-23 interferes also affects SF3B1 thermostability and interferes with spliceosome assembly after intron engagement. *A*, chemical structures of WX-02-23, which covalently binds to SF3B1, and the inactive enantiomer WX-02-43. *B*, comparison of relative anti-SF3B1 dot intensities for soluble fractions of different nuclear extract preparations treated with 200 µM WX-02-23, 200 µM inactive enantiomer WX-02 - 23, or 2 µM SSA-917 and heated to the indicated temperatures. For NE-2, only SSA-917 treatment produced a significant increase in the amount of soluble SF3B1 at 50 and 54 °C. *C*, *Left*: Representative denaturing gel image of radiolabeled RNA isolated after *in vitro* splicing reactions with increasing WX-02-23 or WX-02-43 concentrations (0.2–200 µM), DMSO or 2 µM SSA-917 as a control for full inhibition. RNA band identities illustrated to the *left* are (from the *top*) lariat intron intermediate, pre-mRNA substrate, spliced mRNA, lariat intron, and 5′ exon intermediate. *Right*: Splicing efficiency normalized to DMSO control vs. WX-02-23 (*orange*) or WX-02-43 (*brown*) concentration is determined by the intensity of the mRNA band relative to combined intensity of all RNA species. The WX-02-23 data fit to a non-linear regression model in *orange* yields an IC_{50} value of 5.2 µM (90% CI: 3.1–8.6). *D*, native gel analysis of *in vitro* spliceosome assembly with a radiolabeled RNA substrate at the indicated time points in the presence of 200 µM WX-02-23, 200 µM WX-02-43, DMSO or 2 µM SSA analog. Labels at the *left* show the position of spliceosome complex bands as assembly proceeds from E/H - > A - > B - > C. Both WX-02-23 and the SSA-analog halt assembly with an accumulation of an A-like complex between U2 snRNP and the RNA. In all assays, the inactive enantiomer WX-02-43 has no effect. SSA, spliceostatin A.

might also have an impact on DDX42 thermostability. Furthermore, if they share a similar mechanism of action, the natural product derived SF3B1 inhibitors would have the same effect. We investigated the possibility with SSA-917 and WX-02-23. By western blots, we do not observe a significant change in the amount of DDX42 in the soluble fractions of NE-3 and NE-4 with SSA-917 at temperatures near an estimated T_m near 51 °C (Fig. 6*A*). Likewise, WX-02-23 has no effect in NE-3 (Fig. 6*B*). This result comes with the caveat that we were not able to use HDAC-1 as a loading control because both WX-02-23 and WX-02-43 differentially affected the protein's migration, potentially reflecting their reactive propensities. Because our DDX42 antibody detects a significant non-specific band, dot blotting was not possible. Coincidentally, the non-specific bands migrate at the same position as SF3B1 and its thermostability differs with the inhibitors. A sequence alignment of the DDX42 antigen (amino acids 888–938) identifies a 39 residue stretch within the intrinsically disordered N-terminal domain of SF3B1 that may be similar enough to be recognized (Fig. 6).

Discussion

SF3B1 thermostability and natural product splicing inhibitors

In this study, we developed a thermal shift assay to evaluate spliceosome inhibitor interactions with SF3B1 in the context of the HeLa cell nuclear extract that is used to study splicing and spliceosome assembly *in vitro* (36, 38). Dot blotting, which enabled comparison of replicate measures on the same immunoblot, was critical to observing the small but consistent increase in SF3B1 thermostability in the presence of the splicing inhibitor SSA-917. While the assay does not provide quantitative binding data, we suggest that it can serve as a useful stand-in for assessing binding and complement the functionally relevant test for inhibition of splicing chemistry that is downstream of SF3B1's role in spliceosome assembly.

Compounds derived from three distinct natural product scaffolds (SSA, pladienolide B and herboxidiene) modulate SF3B1 thermostability, which is consistent with a shared pharmacophore and mechanism of action for splicing inhibition. The magnitude of their effect similarly depended on the nuclear extract tested, but SSA and its analog SSA-917 consistently increased SF3B1 thermostability at a given temperature by the highest magnitude. The difference may be due to the slightly higher potency of SSA for *in vitro* splicing inhibition, where SSA's IC_{50} value is 0.07 μM *versus* 0.09 and 0.23 μM for pladienolide B and herboxidiene, respectively, although we tested the compounds at concentrations much higher than their IC_{50} values for splicing inhibition and sufficient to yield no detectable spliced products (39). The compounds share a diene functionality making similar contacts

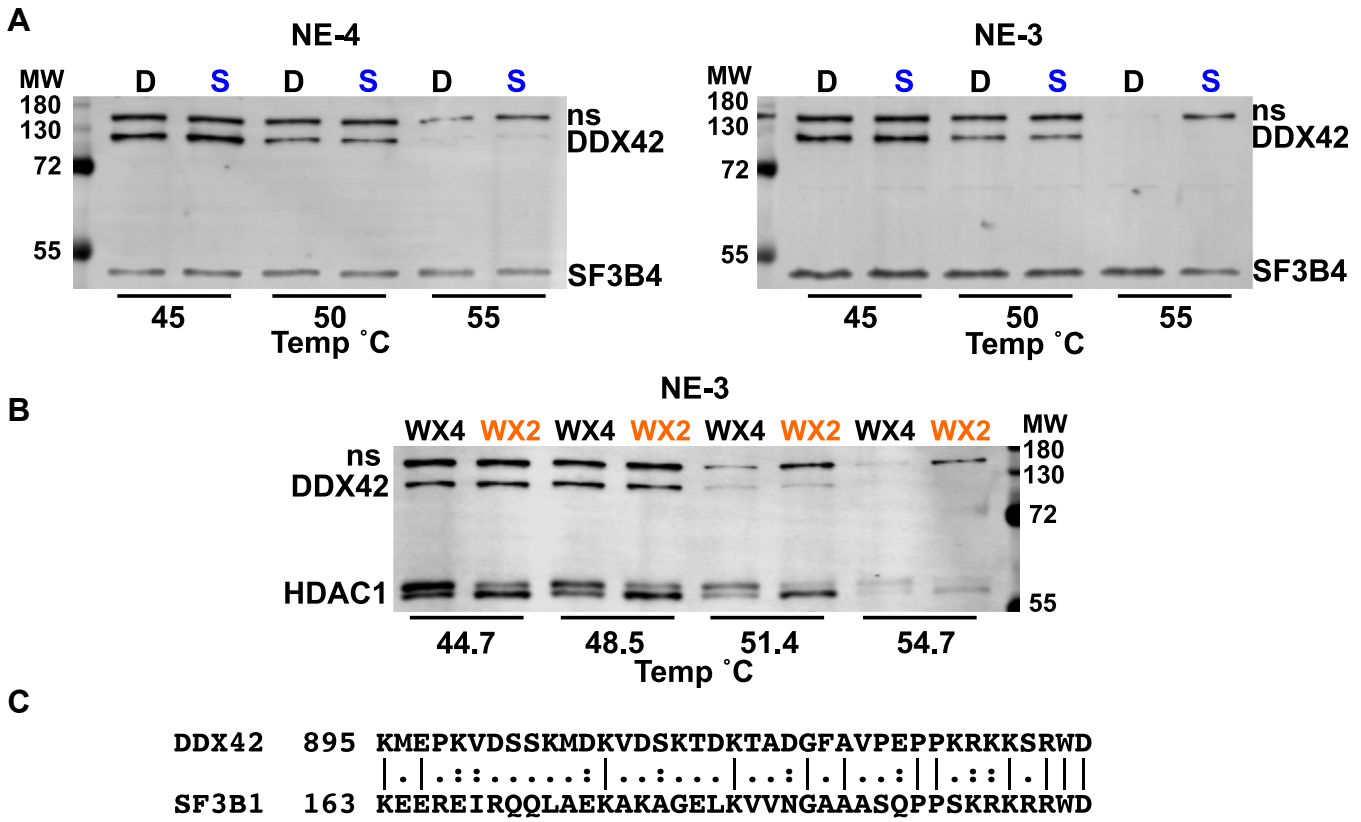

Figure 6. SF3B1 inhibitors have no detected impact on the thermostability of DDX42. *A*, Western analysis of two nuclear extract preparations treated with SSA-917 (S) or DMSO (D) as described in Figure 1*B*. Blots were probed with anti-DDX42 and anti-SF3B4 as a loading control. *B*, as described in (*A*), except using WX-02-23 (WX2) WX-02-43 (WX4) and anti-HDAC1 as an attempted loading control. *C*, similarity between the DDX42 antigen and a region of SF3B1 that may explain the ~155 kD non-specific band identified by the DDX42 antibody that exhibits differential thermostability with the inhibitors. SSA, spliceostatin A.

within the SF3B1 binding site, but their interactions with SF3B1 outside the pocket differ (27–29). For example, SSA has a unique covalent interaction with cysteine 26 of PHF5A that may further influence SF3B1 thermostability (28). The shared aliphatic tail of pladienolide B and herboxidiene contact a completely different surface of SF3B1, with no evidence of covalent linkage. Future examination of the structure activity relationship of different inhibitor contacts relative to SF3B1 thermostability has the potential to explain how different analogs could yield different splicing outcomes in cells in conjunction with the wide variability of introns. Indeed, multiple analogs of SSA have been reported to differentially alter certain splicing events (40).

While employing different nuclear extract preparations in our studies, we discovered that SF3B1 thermostability is also affected by a yet to be identified factor. In some extracts, SF3B1 thermostability is on its own much lower and the impact of inhibitor addition is more profound. Although overall protein/nucleic acid concentration can explain some of the effect, other factors must contribute. One correlation we see relates to the proficiency of the extract for splicing. The SF3B1 in extracts with good splicing efficiency exhibits higher thermostability, while extracts with low SF3B1 thermostability have little to no splicing activity. The corollary of high SF3B1 stability tracking with high splicing efficiency does not hold. This may be expected because dozens of spliceosome components must all be functional to promote splicing, not just SF3B1. The complexity of nuclear extract presents many challenges to teasing out the factors that impact splicing efficiency. SF3B1 thermostability may represent a handhold for characterizing the specific factors that modulate its contributions.

SF3B1 thermostability is likely influenced by its interactions with other components of U2 snRNP and/or the conformation of the large HEAT-repeat domain. We know that the interactions vary among extracts based on, for example, the proportion of SF3B1 in complexes that differentially migrate in glycerol gradients (41, 42). Our group also reported evidence for both temperature and an ATP-dependent factor affecting inhibitor interactions with SF3B1, which we hypothesized modulate the probability of it adopting an open vs. closed conformation (30). With these observations in mind, it is tempting to speculate that SF3B1 is more thermostable when functionally associated with U2 snRNP in an open conformation. In this case, inhibitor binding can only provide a small degree of additional stabilization. In contrast, SF3B1 that is not associated with U2 snRNP may be less thermostable as it fluctuates between open and closed states. By supporting the open state, inhibitor binding to the disassociated SF3B1 would therefore has a larger impact on overall thermostability. We are actively working to test this hypothesis.

One aim of this study is to understand the paradoxical behavior of iHB, which has no effect on *in vitro* splicing efficiency, but antagonizes all three natural product splicing inhibitors (16, 30). For example, 5 μM iHB rescues 50% of splicing that is completely inhibited with 1 μM SSA. The increase in SF3B1 thermostability with iHB is consistent with its binding in the same pocket in SF3B1, regardless of the altered carboxyl group of herboxidiene. The results further implicate interactions between the carboxyl group and residues at the hinge of SF3B1 as being critical to inhibitor mechanism. Other SF3B1 inhibitor analogs also have been shown to have antagonistic properties (43), and thermostability could similarly prove valuable for investigating their mechanism of action.

A new SF3B1 splicing inhibitor

Finally, our investigation of WX-02-23 shows that a covalent ligand modifying SF3B1 near the natural product binding pocket inhibits *in vitro* spliceosome assembly at the same stage and similarly increases SF3B1 thermostability. Together these results highlight the critical nature of the region for SF3B1's role in splicing, and its drugability. Proteomic interaction studies showed that WX-02-23 increases SF3B1 interactions with the protein DDX42 (37). DDX42 was initially identified as a component of the free SF3B complex, but not the U2 snRNP, and proposed to regulate SF3B in addition to the snRNP (44). If stabilizing DDX42 interactions with SF3B1 interferes with U2 snRNP assembly, the spliceosome A-complex would not assemble in the presence of WX-02-23. The drug might also be predicted to affect DDX42 thermostability. Our results show that WX-02-23 does not block U2 snRNP's interaction with an intron, but it halts further assembly similar to the natural product SF3B1 inhibitors. We also see no impact of WX-02-23 or SSA-917 on DDX42 thermostability, which does not support a change in DDX42 interactions with SF3B1, although it also does not rule it out. How interactions with DDX42 impinge on SF3B1 function at this stage is not clear, but a recent cryo-EM model shows it bound to U2 snRNP concomitantly with SF3B in a manner that is both similar to and mutually exclusive of the homologous RNA-dependent ATPase DDX46 (45). The Cravatt group reported that DDX42 preferentially crosslinks to the branch point region of introns, which in combination with our spliceosome assembly data, raises the possibility that it functions as a paralog of DDX46.

Method

SF3B1 inhibitors

Synthesis and characterization of SSA, pladienolide B, herboxidiene analogs, WX-02-23 and WX-02-43 were previously reported (37, 46–49). Synthesis and characterization of SSA-917 will be reported separately. All compounds are stored at 10 to 50 mM in DMSO and diluted in water prior to use.

HeLa nuclear extract preparation

HeLa nuclear extract was prepared as previously described (50) from HeLa S3 cells cultivated in DMEM/F-12 medium and 5% (v/v) newborn calf serum. Briefly, cells grown in suspension were harvested by centrifugation and washed twice with cold PBS and twice with 10 mM Tris pH 7.9, 10 mM KCl, 1.5 mM MgCl2, 0.5 mM DTT, supplemented with cOmplete Protease Inhibitor Cocktail (469313200, Roche). The cells were swelled in 2X volume of the same buffer for 10 min and the

plasma membrane disrupted with a glass dounce homogenizer. Nuclei were pelleted and resuspended in 0.5X volume 20 mM Tris pH 7.9, 0.02 M KCl, 1.5 mM $MgCl_2$, 25% glycerol, 0.5 mM DTT supplemented with cOmplete Protease Inhibitor Cocktail. To precipitate chromatin, 0.5X volume of 20 mM Tris pH 7.9, 1.2 M KCl, 1.5 mM $MgCl_2$, 25% glycerol, and 0.5 mM DTT supplemented with cOmplete Protease Inhibitor Cocktail was added dropwise with stirring. After centrifugation, the soluble fraction was dialyzed into NE Buffer (20 mM Tris pH 7.9, 0.1 M KCl, 0.2 mM EDTA, 20% glycerol, and 0.5 mM DTT). Precipitated material was removed by centrifugation, and aliquots of the extract were flash frozen on dry ice and stored at −70 °C.

Thermal shift assay

HeLa nuclear extract diluted in NE Buffer was incubated with drug or DMSO for 10 min at 30 °C and then transferred into PCR tubes in 10 µl aliquots. The tubes were heated in a thermal cycler for 3 min at temperatures ranging from 40 to 65 °C, cooled at room temperature for 3 min, and then placed on ice. The samples were diluted to a final volume of 50 to 100 µl with NE Buffer and transferred to 1.7 ml microfuge tubes. Insoluble protein was pelleted by centrifugation at 17,000*g* for 30 min at 4 °C. Supernatant containing soluble protein was transferred to tubes or a 96-well plate and aliquots were analyzed by blotting immediately or stored at −20 °C.

Dot blots

Immobilon-FL 045 µm PVDF membrane (IPL00010, Millipore) was activated with methanol and equilibrated in 10 mM Tris pH 7.5, 150 mM NaCl, 0.05 Tween-20 (1X TBS-T). The membrane was placed on two layers of damp Whatman 3 MM filter paper (3030–392, Whatman) and assembled in a 96-well Minifold I Dot Blot System (349–46321, Whatman). Soluble protein fractions were loaded into wells by multichannel pipette and vacuum applied to pull liquid through the membrane. The wells were then rinsed with NE Buffer with vacuum. After a short drying time, the membrane was incubated with agitation in 1X TBS-T with 1% non-fat dry milk for 1 hour at room temperature. Primary antibody (anti-SF3B1, 27684-1-AP, Proteintech, RRID:AB_2880946, 1:7000 dilution) was added directly to the milk solution, and the membrane incubated overnight at 4 °C with agitation. The blots were washed with 1X TBS-T for 5 min three times, followed by incubation with secondary antibody (IRDye 680RD Donkey anti-Rabbit IgG, 926–68073, LICOR, RRID:AB_10954442, 1:15,0000 dilution) in 1X TBS-T with 1% non-fat dry milk for 1 h at room temperature. Antibody specificity was determined by the manufacturer. The blots were washed again and imaged with the Odyssey Infrared Imaging System (LI-COR Biosciences). Dot blot images were quantified from using LI-COR Image Studio Lite and relative intensities expressed as signal divided by the average signal of the lowest temperature treatment for the extract. T_m (IC_{50}) values were determined by nonlinear regression using the default [Inhibitor] vs. response – Variable slope model with $1/Y^2$ weighting in GraphPad Prism version 10.3.1 for Mac, GraphPad Software, www.graphpad.com. Curve fits were compared by the Extra sum of squares F test to determine *p*-values for differences in T_m.

Western blot

Soluble protein samples were prepared in 5x Laemmli buffer (62.5 mM Tris, 25% glycerol, 6.25% SDS, 0.1% bromophenol blue, 5% beta-mercaptoethanol) and heated at 95 °C for 1 min prior separation on 10% acrylamide gels for SDS-PAGE. Gels were transferred to Immobilon-FL PVDF in 25 mM Tris, 192 mM glycine, 20% (v/v) methanol, 0.05% SDS with a Bio-Rad Mini Trans-Blot Cell. The membranes were probed and imaged as described for dot blots except that anti-HDAC1 (H-51) rabbit polyclonal (SC-7872, Santa Cruz Biotech, AB_2279709, 1:3000 dilution), anti-DDX42 rabbit polyclonal A303–354A, Bethyl Laboratories, RRID:AB_10953655, 1:2000) or anti-SF3B4 (G3) mouse monoclonal (sc-365571, Santa Cruz Biotech, RRID:AB_10851485, 1:1000 dilution) was included as primary antibody and, where appropriate, (IRDye 800C2 Donkey anti-mouse IgG, 925–32212, LICOR, RRID:AB_2716622, 1:15,0000 dilution) included as secondary antibody. Antibody specificity was determined by the manufacturer. Bands were quantified from with LI-COR Image Studio Lite. SF3B1 signal for a given temperature was first normalized to HDAC1 as a loading control, and relative intensities expressed as signal divided by the average signal of the lowest temperature treatment for the extract. Data were plotted and analyzed as described for dot blots.

In vitro *splicing assays*

Radiolabeled pre-mRNA substrate (5–10 nM) was incubated at 30 °C for 60 min in 40% HeLa cell nuclear extract supplemented with 60 mM potassium glutamate, 2 mM magnesium acetate, 2 mM ATP, 5 mM creatine phosphate, 0.1 mg/ml tRNA, and increasing concentrations of compounds solved in DMSO or DMSO alone. The reactions were stopped by addition of and the RNA isolated by extraction with 25:24:1 phenol:cholorform:isoamyl alcohol and ethanol precipitation. RNA species were separated by denaturing polyacrylamide gel electrophoresis and visualized by phosphorimaging (Typhoon, Molecular Dynamics). Individual bands were quantified with FIJI. Splicing efficiency is calculated as the amount of mRNA relative to total RNA and normalized to a DMSO control reaction. Values from three independent measurements were graphed and IC_{50} values determined by nonlinear regression using the default [Inhibitor] vs. response - Variable slope model in GraphPad Prism version 10.3.1 for Mac, GraphPad Software, www.graphpad.com.

Native gel analysis

Aliquots of *in vitro* splicing reactions were taken at different time intervals and combined with one volume of native loading buffer (20 mM Tris base, 20 mM glycine, 25% (v/v) glycerol, 0.05% (w/v) cyan blue, 0.05% (w/v) bromophenol blue, 1 mg/ml heparin sulfate) for loading on a horizontal 2.1% (w/v) low-melt agarose gel in 20 mM Tris, 20 mM glycine running buffer.

Gels were run at 72 V for 3 h 50 min, vacuum-dried onto Whatman 3 MM filter paper for 45 min at 65 °C, and visualized by phosphorimaging (Typhoon, Molecular Dynamics).

Data availability

All data described are contained within the article.

Author contributions—M. S. J. and A. N. A. conceptualization, M. S. J. data curation, M. S. J. formal analysis, M. S. J. funding acquisition, M. S. J. and A. N. A. investigation, M. S. J. and A. N. A. methodology, M. S. J. project administration, M. S. J. supervision, M. S. J. and A. N. A. validation, M. S. J. and A. N. A. visualization, M. S. J. and A. N. A. writing–original draft; M. S. J. writing–review & editing; G. C. R., A. K. G., B. F. C., and B. M. resources; A. K. G. and B. F. C. supervision.

Funding and additional information—This work was supported by National Institutes of Health grant R01GM72649 to MSJ and AKG and R35CA231991 to BFC. AA was further supported by a university-sponsored Initiative to Maximize Student Development fellowship.

Conflict of interest—The authors declare that they have no conflicts of interest with the contents of this article.

Abbreviations—The abbreviations used are: MDS, myelodysplastic syndrome; PP2A, protein phosphatase 2A; SF3B, Splicing factor 3B; SSA, spliceostatin A; U2-Snrp, U2 small nuclear ribonucleoprotein.

References

1. Kramer, A., Gruter, P., Groning, K., and Kastner, B. (1999) Combined biochemical and electron microscopic analyses reveal the architecture of the mammalian U2 snRNP. *J. Cell Biol.* **145**, 1355–1368
2. Quesada, V., Conde, L., Villamor, N., Ordonez, G. R., Jares, P., Bassaganyas, L., *et al.* (2011) Exome sequencing identifies recurrent mutations of the splicing factor SF3B1 gene in chronic lymphocytic leukemia. *Nat. Genet.* **44**, 47–52
3. Yoshida, K., Sanada, M., Shiraishi, Y., Nowak, D., Nagata, Y., Yamamoto, R., *et al.* (2011) Frequent pathway mutations of splicing machinery in myelodysplasia. *Nature* **478**, 64–69
4. Papaemmanuil, E., Cazzola, M., Boultwood, J., Malcovati, L., Vyas, P., Bowen, D., *et al.* (2011) Somatic SF3B1 mutation in myelodysplasia with ring sideroblasts. *N. Engl. J. Med.* **365**, 1384–1395
5. Harbour, J. W., Roberson, E. D., Anbunathan, H., Onken, M. D., Worley, L. A., and Bowcock, A. M. (2013) Recurrent mutations at codon 625 of the splicing factor SF3B1 in uveal melanoma. *Nat. Genet.* **45**, 133–135
6. Darman, R. B., Seiler, M., Agrawal, A. A., Lim, K. H., Peng, S., Aird, D., *et al.* (2015) Cancer-associated SF3B1 hotspot mutations induce cryptic 3′ splice site selection through use of a different branch point. *Cell Rep.* **13**, 1033–1045
7. Alsafadi, S., Houy, A., Battistella, A., Popova, T., Wassef, M., Henry, E., *et al.* (2016) Cancer-associated SF3B1 mutations affect alternative splicing by promoting alternative branchpoint usage. *Nat. Commun.* **7**, 10615
8. Liu, Z., Yoshimi, A., Wang, J., Cho, H., Chun-Wei Lee, S., Ki, M., *et al.* (2020) Mutations in the RNA splicing factor SF3B1 promote tumorigenesis through MYC stabilization. *Cancer Discov.* **10**, 806–821
9. Sakai, Y., Yoshida, T., Ochiai, K., Uosaki, Y., Saitoh, Y., Tanaka, F., *et al.* (2002) GEX1 compounds, novel antitumor antibiotics related to herboxidiene, produced by Streptomyces sp. I. Taxonomy, production, isolation, physicochemical properties and biological activities. *J. Antibiot. (Tokyo)* **55**, 855–862
10. Mizui, Y., Sakai, T., Iwata, M., Uenaka, T., Okamoto, K., Shimizu, H., *et al.* (2004) Pladienolides, new substances from culture of Streptomyces platensis Mer-11107. III. In vitro and in vivo antitumor activities. *J. Antibiot. (Tokyo)* **57**, 188–196
11. Nakajima, H., Sakaguchi, K., Fujiwara, I., Mizuta, M., Tsuruga, M., Magae, J., *et al.* (2007) Apoptosis and inactivation of the PI3-kinase pathway by tetrocarcin A in breast cancers. *Biochem. Biophys. Res. Commun.* **356**, 260–265
12. Kotake, Y., Sagane, K., Owa, T., Mimori-Kiyosue, Y., Shimizu, H., Uesugi, M., *et al.* (2007) Splicing factor SF3b as a target of the antitumor natural product pladienolide. *Nat. Chem. Biol.* **3**, 570–575
13. Hasegawa, M., Miura, T., Kuzuya, K., Inoue, A., Won Ki, S., Horinouchi, S., *et al.* (2011) Identification of SAP155 as the target of GEX1A (Herboxidiene), an antitumor natural product. *ACS Chem. Biol.* **6**, 229–233
14. Nakajima, H., Hori, Y., Terano, H., Okuhara, M., Manda, T., Matsumoto, S., *et al.* (1996) New antitumor substances, FR901463, FR901464 and FR901465. II. Activities against experimental tumors in mice and mechanism of action. *J. Antibiot. (Tokyo)* **49**, 1204–1211
15. Roybal, G. A., and Jurica, M. S. (2010) Spliceostatin A inhibits spliceosome assembly subsequent to prespliceosome formation. *Nucleic Acids Res.* **38**, 6664–6672
16. Effenberger, K. A., Urabe, V. K., Prichard, B. E., Ghosh, A. K., and Jurica, M. S. (2016) Interchangeable SF3B1 inhibitors interfere with pre-mRNA splicing at multiple stages. *RNA* **22**, 350–359
17. Folco, E. G., Coil, K. E., and Reed, R. (2011) The anti-tumor drug E7107 reveals an essential role for SF3b in remodeling U2 snRNP to expose the branch point-binding region. *Genes Dev.* **25**, 440–444
18. Corrionero, A., Minana, B., and Valcarcel, J. (2011) Reduced fidelity of branch point recognition and alternative splicing induced by the anti-tumor drug spliceostatin A. *Genes Dev.* **25**, 445–459
19. Obeng, E. A., Chappell, R. J., Seiler, M., Chen, M. C., Campagna, D. R., Schmidt, P. J., *et al.* (2016) Physiologic expression of Sf3b1(K700E) causes impaired erythropoiesis, aberrant splicing, and sensitivity to therapeutic spliceosome modulation. *Cancer Cell* **30**, 404–417
20. Seiler, M., Yoshimi, A., Darman, R., Chan, B., Keaney, G., Thomas, M., *et al.* (2018) H3B-8800, an orally available small-molecule splicing modulator, induces lethality in spliceosome-mutant cancers. *Nat. Med.* **24**, 497–504
21. Steensma, D. P., Wermke, M., Klimek, V. M., Greenberg, P. L., Font, P., Komrokji, R. S., *et al.* (2019) Results of a clinical trial of H3B-8800, a splicing modulator, in patients with myelodysplastic syndromes (MDS), acute myeloid leukemia (AML) or chronic myelomonocytic leukemia (CMML). *Blood* **134**, 673
22. Maji, D., Grossfield, A., and Kielkopf, C. L. (2019) Structures of SF3b1 reveal a dynamic Achilles heel of spliceosome assembly: implications for cancer-associated abnormalities and drug discovery. *Biochim. Biophys. Acta Gene Regul. Mech.* **1862**, 194440
23. Zhang, Z., Will, C. L., Bertram, K., Dybkov, O., Hartmuth, K., Agafonov, D. E., *et al.* (2020) Molecular architecture of the human 17S U2 snRNP. *Nature* **583**, 310–313
24. Rauhut, R., Fabrizio, P., Dybkov, O., Hartmuth, K., Pena, V., Chari, A., *et al.* (2016) Molecular architecture of the Saccharomyces cerevisiae activated spliceosome. *Science* **353**, 1399–1405
25. Yan, C., Wan, R., Bai, R., Huang, G., and Shi, Y. (2016) Structure of a yeast activated spliceosome at 3.5 A resolution. *Science* **353**, 904–911
26. Plaschka, C., Lin, P. C., Charenton, C., and Nagai, K. (2018) Prespliceosome structure provides insights into spliceosome assembly and regulation. *Nature* **559**, 419–422
27. Cretu, C., Agrawal, A. A., Cook, A., Will, C. L., Fekkes, P., Smith, P. G., *et al.* (2018) Structural basis of splicing modulation by antitumor macrolide compounds. *Mol. Cell* **70**, 265–273e8
28. Cretu, C., Gee, P., Liu, X., Agrawal, A., Nguyen, T. V., Ghosh, A. K., *et al.* (2021) Structural basis of intron selection by U2 snRNP in the presence of covalent inhibitors. *Nat. Commun.* **12**, 4491
29. Finci, L. I., Zhang, X., Huang, X., Zhou, Q., Tsai, J., Teng, T., *et al.* (2018) The cryo-EM structure of the SF3b spliceosome complex bound to a splicing modulator reveals a pre-mRNA substrate competitive mechanism of action. *Genes Dev.* **32**, 309–320
30. Gamboa Lopez, A., Allu, S. R., Mendez, P., Chandrashekar Reddy, G., Maul-Newby, H. M., Ghosh, A. K., *et al.* (2021) Herboxidiene features

that mediate conformation-dependent SF3B1 interactions to inhibit splicing. *ACS Chem. Biol.* **16**, 520–528
31. Liang, W. W., and Cheng, S. C. (2015) A novel mechanism for Prp5 function in prespliceosome formation and proofreading the branch site sequence. *Genes Dev.* **29**, 81–93
32. Xu, Y. Z., and Query, C. C. (2007) Competition between the ATPase Prp5 and branch region-U2 snRNA pairing modulates the fidelity of spliceosome assembly. *Mol. Cell* **28**, 838–849
33. Teng, T., Tsai, J. H., Puyang, X., Seiler, M., Peng, S., Prajapati, S., *et al.* (2017) Splicing modulators act at the branch point adenosine binding pocket defined by the PHF5A-SF3b complex. *Nat. Commun.* **8**, 15522
34. Martinez Molina, D., Jafari, R., Ignatushchenko, M., Seki, T., Larsson, E. A., Dan, C., *et al.* (2013) Monitoring drug target engagement in cells and tissues using the cellular thermal shift assay. *Science* **341**, 84–87
35. Jafari, R., Almqvist, H., Axelsson, H., Ignatushchenko, M., Lundbäck, T., Nordlund, P., *et al.* (2014) The cellular thermal shift assay for evaluating drug target interactions in cells. *Nat. Protoc.* **9**, 2100–2122
36. Padgett, R. A., Hardy, S. F., and Sharp, P. A. (1983) Splicing of adenovirus RNA in a cell-free transcription system. *Proc. Natl. Acad. Sci. U. S. A.* **80**, 5230–5234
37. Lazear, M. R., Remsberg, J. R., Jaeger, M. G., Rothamel, K., Her, H. L., DeMeester, K. E., *et al.* (2023) Proteomic discovery of chemical probes that perturb protein complexes in human cells. *Mol. Cell* **83**, 1725–1742. e12
38. Ruskin, B., Krainer, A. R., Maniatis, T., and Green, M. R. (1984) Excision of an intact intron as a novel lariat structure during pre-mRNA splicing in vitro. *Cell* **38**, 317–331
39. Effenberger, K. A., Anderson, D. D., Bray, W. M., Prichard, B. E., Ma, N., Adams, M. S., *et al.* (2014) Coherence between cellular responses and in vitro splicing inhibition for the anti-tumor drug pladienolide B and its analogs. *J. Biol. Chem.* **289**, 1938–1947
40. Vigevani, L., Gohr, A., Webb, T., Irimia, M., and Valcarcel, J. (2017) Molecular basis of differential 3' splice site sensitivity to anti-tumor drugs targeting U2 snRNP. *Nat. Commun.* **8**, 2100
41. Behrens, S. E., Tyc, K., Kastner, B., Reichelt, J., and Luhrmann, R. (1993) Small nuclear ribonucleoprotein (RNP) U2 contains numerous additional proteins and has a bipartite RNP structure under splicing conditions. *Mol. Cell Biol.* **13**, 307–319
42. Brosi, R., Hauri, H. P., and Kramer, A. (1993) Separation of splicing factor SF3 into two components and purification of SF3a activity. *J. Biol. Chem.* **268**, 17640–17646
43. Shi, Y., Bray, W., Smith, A. J., Zhou, W., Calaoagan, J., Lagisetti, C., *et al.* (2020) An exon skipping screen identifies antitumor drugs that are potent modulators of pre-mRNA splicing, suggesting new therapeutic applications. *PLoS One* **15**, e0233672
44. Will, C. L., Urlaub, H., Achsel, T., Gentzel, M., Wilm, M., and Luhrmann, R. (2002) Characterization of novel SF3b and 17S U2 snRNP proteins, including a human Prp5p homologue and an SF3b DEAD-box protein. *EMBO J.* **21**, 4978–4988
45. Yang, F., Bian, T., Zhan, X., Chen, Z., Xing, Z., Larsen, N. A., *et al.* (2023) Mechanisms of the RNA helicases DDX42 and DDX46 in human U2 snRNP assembly. *Nat. Commun.* **14**, 897
46. Ghosh, A. K., and Li, J. (2011) A stereoselective synthesis of (+)-herboxidiene/GEX1A. *Org. Lett.* **13**, 66–69
47. Ghosh, A. K., and Anderson, D. D. (2012) Enantioselective total synthesis of pladienolide B: a potent spliceosome inhibitor. *Org. Lett.* **14**, 4730–4733
48. Ghosh, A. K., and Chen, Z. H. (2013) Enantioselective syntheses of FR901464 and spliceostatin A: potent inhibitors of spliceosome. *Org. Lett.* **15**, 5088–5091
49. Ghosh, A. K., Allu, S. R., Reddy, G. C., Lopez, A. G., Mendez, P., and Jurica, M. S. (2021) Design and synthesis of herboxidiene derivatives that potently inhibit in vitro splicing. *Org. Biomol. Chem.* **19**, 1365–1377
50. Dignam, J. D., Lebovitz, R. M., and Roeder, R. D. (1983) Accurate transcription initiation by RNA polymerase II in a soluble extract from isolated mammalian nuclei. *Nucleic Acids Res.* **11**, 1475–1489